Journal of Inorganic Biochemistry 132 (2014) 21–29

Contents lists available at ScienceDirect

Journal of Inorganic Biochemistry

journal homepage: www.elsevier.com/locate/jinorgbio

Manganese(II) complexes with thiosemicarbazones as potential anti-*Mycobacterium tuberculosis* agents

Carolina G. Oliveira [a], Pedro Ivo da S. Maia [b], Paula C. Souza [c], Fernando R. Pavan [c], Clarice Q.F. Leite [c], Rommel B. Viana [a], Alzir A. Batista [d], Otaciro R. Nascimento [e], Victor M. Deflon [a,*]

[a] Instituto de Química de São Carlos, Universidade de São Paulo, 13566-590 São Carlos, SP, Brazil
[b] Departamento de Química, Universidade Federal do Triângulo Mineiro, 38025-440 Uberaba, MG, Brazil
[c] Faculdade de Ciências Farmacêuticas, Universidade Estadual Paulista, 14801-902 Araraquara, SP, Brazil
[d] Departamento de Química, Universidade Federal de São Carlos, 13565-905 São Carlos, SP, Brazil
[e] Instituto de Física de São Carlos, Universidade de São Paulo, CP 369, 13560-970 São Carlos, SP, Brazil

ARTICLE INFO

Article history:
Received 30 May 2013
Received in revised form 18 October 2013
Accepted 19 October 2013
Available online 25 October 2013

Keywords:
Manganese(II)
Thiosemicarbazones
Anti-*Mycobacterium tuberculosis* activity
Catalase peroxidase

ABSTRACT

Through a systematic variation on the structure of a series of manganese complexes derived from 2-acetylpyridine-N(4)-R-thiosemicarbazones (Hatc-R), structural features have been investigated with the aim of obtaining complexes with potent anti-*Mycobacterium tuberculosis* activity. The analytical methods used for characterization included FTIR, EPR, UV–visible, elemental analysis, cyclic voltammetry, magnetic susceptibility measurement and single crystal X-ray diffractometry. Density functional theory (DFT) calculations were performed in order to evaluate the contribution of the thiosemicarbazonate ligands on the charge distribution of the complexes by changing the peripheral groups as well as to verify the Mn–donor atoms bond dissociation predisposition. The results obtained are consistent with the mono-anionic *N,N,S*-tridentate coordination of the thiosemicarbazone ligands, resulting in octahedral complexes of the type $[Mn(atc\text{-}R)_2]$, paramagnetic in the extension of 5 unpaired electrons, whose EPR spectra are consistent for manganese(II). The electrochemical analyses show two nearly reversible processes, which are influenced by the peripheral substituent groups at the N4 position of the atc-R^{1-} ligands. The minimal inhibitory concentration (MIC) of these compounds against *M. tuberculosis* as well as their in vitro cytotoxicity on VERO and J774A.1 cells (IC_{50}) was determined in order to find their selectivity index (SI) ($SI = IC_{50} / MIC$). The results evidenced that the compounds described here can be considered as promising anti-*M. tuberculosis* agents, with SI values comparable or better than some commercial drugs available for the *tuberculosis* treatment.

1. Introduction

The World Health Organization (WHO) estimates that tuberculosis (TB) has become one of the deadliest global emergencies due to the widespread existence of multiple drug resistant strains of *Mycobacterium tuberculosis* (MTB), frequently caused by limited health care system resources combined with the increasing numbers of HIV/AIDS [1]. In addition, a number of anti-TB drugs may be discontinued in a few years due to the expanding number of multidrug resistant TB (MDR-TB) and extensively drug-resistant (XDR-TB) cases [2]. Therefore, there is a serious need for new anti-MTB agents that target new biochemical pathways and treat drug resistant forms of the disease [3,4].

Catalase–peroxidase (CP or KatG) is a heme protein that exhibits both catalase and peroxidase activities and plays a crucial role in defending against oxidative stress generated by aerobic oxygen metabolism or phagocytic attack from macrophages or neutrophils [5,6]. In MTB the KatG is responsible for the conversion of Mn(II) to Mn(III) in metalloenzymes containing manganese in active sites and has attracted special attention due to its participation in mycobacterial virulence [7]. On the other hand, KatG is also important for the activation of the pro-drug isoniazid (INH) [8]. Most of the INH resistance is associated with KatG structural gene alterations resulting in KatG mutant enzymes with reduced ability to form activated INH-intermediates [8,9]. It has been shown that both KatG and Mn complexes are able to oxidize isoniazid and form the active isonicotinoyl–NAD adduct [7]. Therefore, manganese complexes have been proposed as an alternative oxidant mimicking the activity of KatG and thus providing a non-enzymatic isoniazid activation method [6,7].

In this context, it was demonstrated that the redox reversible metal complex $[Fe^{II}(CN)_5(INH)]^{3-}$ [10] containing the pro-drug was able to overcome the drug resistance. This complex presents a minimal

* Corresponding author.
E-mail address: deflon@iqsc.usp.br (V.M. Deflon).

0162-0134/$ – see front matter © 2013 Elsevier Inc. All rights reserved.
http://dx.doi.org/10.1016/j.jinorgbio.2013.10.011

inhibitory concentration (MIC, defined as the lowest concentration resulting in 90% of growth inhibition of the bacteria) value similar to that of free isoniazid as well as a good selectivity index. Its mechanism of action is supposed to be independent of the KatG enzyme since it is active against INH-resistant MTB [10]. Similar to iron complexes, manganese species also take part in many biological redox processes and can easily achieve different oxidation states.

Thiosemicarbazones (TSCs) are of great interest both in chemistry and biology, especially due to their antiparasital [11], antitumor [12–14] and antibacterial activities [15]. Moreover, the biological properties of the TSCs are often referred to their complex formation since it can increase the biological activity by forming chelates with metal ions [12,16,17]. Previous studies showed that V(IV,V) complexes [18] and octahedral Ni(II) complexes [19] derived from 2-acetylpyridine thiosemicarbazones possess anti-MTB activity that can be increased by structural modifications on the thiosemicarbazone moiety.

Literature data dealing with manganese complexes with thiosemicarbazones [20,21] have evaluated the biological activity of these compounds against cancer cells and some bacteria other than MTB. Believing in the high potential of such compounds as anti-MTB agents and also contributing to their full characterization, here we describe the preparation of manganese complexes derived from 2-acetylpyridine-thiosemicarbazones, their characterization by diverse methods as well as the study of their anti-MTB activity and cytotoxicity.

2. Experimental

2.1. Materials

2-Acetylpyridine, thiosemicarbazide, 4-methyl-3-thiosemicarbazide, 4-ethyl-3-thiosemicarbazide, 4-phenyl-3-thiosemicarbazide and analytical reagent grade chemicals and solvents were obtained commercially and used without further purification. 4-Cyclohexyl-3-thiosemicarbazide and 3-morpholynylthiosemicarbazide were prepared as previously described [3,22]. The ligands Hatc, Hatc-Me, Hatc-Et, Hatc-Ch, Hatc-Ph and Hatc-Mf were prepared by refluxing equimolar ethanolic solutions containing the desired thiosemicarbazide (10 mmol) and 2-acetylpyridine (10 mmol) for 1 h, as reported elsewhere [18,23].

2.2. Instruments

FTIR spectra were measured as KBr pellets on a Shimadzu IR Prestige-21 spectrophotometer between 400 and 4000 cm^{-1}. Elemental analyses were determined using a Perkin-Elmer CHN 2400 equipment. EPR spectra were collected on an X-band BrukerER-580 spectrometer equipped with an Oxford low temperature system at 6 K. The spectra were simulated with the Symphonia program from BRUKER. The measurement conditions include microwave frequency of 9.476 GHz, modulation frequency and amplitude of 100 kHz and 0.4 mT, respectively, magnetic field scan range of 5–605 mT, gain of 45 dB, microwave power of 2.5 mW, time constant of 20.48 ms and conversion time of 81.92 ms. The quantification of the two species in the EPR spectra of some of the complexes was estimated by double integration of each spectrum. Magnetic susceptibilities were measured on a JOHNSON MATTHEY MSB balance at 298 K and converted into the corresponding molar susceptibilities in the usual way [24,25]. Diamagnetic corrections, applied to the molar susceptibilities of the paramagnetic substances, are reported as χ_{diam}. The latter corrections were calculated using the standard Pascal's constants [24,25]. The conductivities of the complexes were measured in CH_2Cl_2 solutions using an Orion Star Series conductometer. UV–visible (UV–vis) spectra were measured with a Shimadzu UV-1800 spectrophotometer in CH_2Cl_2 solutions. The electrochemical experiments were carried out at room temperature in dichloromethane or dimethyl sulfoxide containing 0.1 M tetrabutylammonium perchlorate (PTBA) (Fluka Purum) as supporting electrolyte, using an electro-chemical analyzer μAutolab III or a Bioanalytical Systems Inc. (BAS), model 100BW. The working and auxiliary electrodes were stationary Pt and the reference electrode was Ag/AgCl, a medium in which ferrocene is oxidized at 0.5 V (Fc/Fc^+), carried out with a rate sweep of 100 mV s^{-1}.

2.3. Preparations

The Mn(II) complexes were synthesized by adding 0.25 mmol $MnCl_2 \cdot 2H_2O$ to solutions of 0.5 mmol of the desired ligands in 15 mL of MeOH containing 3 drops of Et_3N. The resulting solutions were stirred for 4 h under reflux. The brown solids precipitated during this time were filtered off, washed with water and dried under vacuum. By slow evaporation of the mother solution of **3**, orange crystals suitable for X-ray diffraction analysis were obtained.

$[Mn(atc)_2]\cdot H_2O$ (**1**$\cdot H_2O$): Yield 0.057 g (48%). Analysis: Found: C, 41.51; H, 4.31; N, 24.55%. Calc. for $C_{16}H_{20}N_8OS_2Mn$: C, 41.82; H, 4.39; N, 24.40%. IR (ν_{max}/cm^{-1}): 3373, 3124 ν(N–H), 1624, 1593, 1548 ν(C═N) + ν(C═C), 989 ν(N–N), 773 ν(C–S). UV–Vis in 3.39×10^{-5} M CH_2Cl_2 solution [λ_{max} (, M^{-1} cm^{-1})]: 392.00 nm (18466), 296.00 nm (20324). Molar conductivity (1×10^{-3} M dichloromethane): 0.24 μS cm^{-1}. μ_{eff}: 6.03 BM.

$[Mn(atc\text{-}Me)_2]$ (**2**): Yield 0.062 g (53%). Analysis: Found: C, 45.42; H, 4.72; N, 23.84%. Calc. for $C_{18}H_{22}N_8S_2Mn$: C, 46.05; H, 4.73; N, 23.88%. IR (ν_{max}/cm^{-1}): 3329 ν(N–H), 1591, 1548, 1506 ν(C═N) + ν(C═C), 972 ν(N–N), 781 ν(C–S). UV–Vis in 1.06×10^{-5} M CH_2Cl_2 solution [λ_{max} (, M^{-1} cm^{-1})]: 397.5 nm (78301), 309.0 nm (63962). Molar conductivity (1×10^{-3} M dichloromethane): 0.24 μS cm^{-1}. μ_{eff}: 5.90 BM.

$[Mn(atc\text{-}Et)_2]$ (**3**): Yield 0.080 g (64%). Analysis: Found: C, 48.15; H, 5.31; N, 22.51%. Calc. for $C_{20}H_{26}N_8S_2Mn$: C, 48.28; H, 5.27; N, 22.54%. IR (ν_{max}/cm^{-1}): 3203 ν(N–H), 1593, 1550, 1517 ν(C═N) + ν(C═C), 972 ν(N–N), 780 ν(C–S). UV–Vis in 2.21×10^{-5} M CH_2Cl_2 solution [λ_{max} (, M^{-1} cm^{-1})]: 399.00 nm (20814), 309.50 nm (27511). Molar conductivity (1×10^{-3} M dichloromethane): 0.08 μS cm^{-1}. μ_{eff}: 6.09 BM.

$[Mn(atc\text{-}Ch)_2]$ (**4**): Yield: 0.092 g (61%). Analysis: Found: C, 55.67; H, 6.40; N, 18.76%. Calc. for $C_{28}H_{38}N_8S_2Mn$: C, 55.52; H, 6.33; N, 18.51%. IR (ν_{max}/cm^{-1}): 3290 ν(N–H), 1591, 1543, 1516 ν(C═N) + ν(C═C), 989 ν(N–N), 773 ν(C–S). UV–Vis in 3.30×10^{-5} M CH_2Cl_2 solution [λ_{max} (, M^{-1} cm^{-1})]: 400.50 nm (25894); 311.50 nm (21121). Molar conductivity (1×10^{-3} M dichloromethane): 0.22 μS cm^{-1}. μ_{eff}: 6.10 BM.

$[Mn(atc\text{-}Ph)_2]$ (**5**): Yield 0.118 g (80%). Analysis: Found: C, 56.37; H, 4.80; N, 18.88%. Calc. for $C_{28}H_{26}N_8S_2Mn$: C, 56.65; H, 4.42; N, 18.89%. IR (ν_{max}/cm^{-1}): 3313 ν(N–H), 1593, 1537, 1494 ν(C═N) + ν(C═C), 987 ν(N–N), 777 ν(C–S). UV–Vis in 1.76×10^{-5} M CH_2Cl_2 solution [λ_{max} (, M^{-1} cm^{-1})]: 415.50 nm (13851), 369.00 nm (26136), 315.50 nm (34545). Molar conductivity (1×10^{-3} M dichloromethane): 0.03 μS cm^{-1}. μ_{eff}: 6.30 BM.

$[Mn(atc\text{-}Mf)_2]$ (**6**): Yield: 0.080 g (55%). Analysis: Found: C, 49.21; H, 4.95; N, 18.75%. Calc. for $C_{24}H_{30}N_8O_2S_2Mn$: C, 49.56; H, 5.20; N, 19.28%. IR (ν_{max}/cm^{-1}): 1593, 1543, 1450 ν(C═N) + ν(C═C), 985 ν(N–N), 788 ν(C–S). UV–Vis in 2.06×10^{-5} M CH_2Cl_2 solution [λ_{max} (, M^{-1} cm^{-1})]: 407.50 nm (1 817), 313.00 nm (12718). Molar conductivity (1×10^{-3} M dichloromethane): 0.14 μS cm^{-1}. μ_{eff}: 6.55 BM.

2.4. Crystal structure determination

Orange crystals were grown by slow evaporation of a MeOH solution of [Mn(atc-Et)$_2$] at room temperature. The data collection was performed using Mo-Kα radiation (λ = 71.073 pm) on a BRUKER APEX II Duo diffractometer. Standard procedures were applied for data reduction and absorption correction. The structures were solved with SHELXS97 using direct methods [26] and all non-hydrogen atoms were refined with anisotropic displacement parameters with SHELXL97 [27]. The hydrogen atoms were calculated at idealized positions using the riding model option of SHELXL97 [27]. Table 1 presents more detailed information about the structure determination.

2.5. Computational methodology

The computational simulations were performed using the Gaussian 09 program [28]. Geometry optimization procedure was carried out with density functional theory (DFT), using the PBE1PBE functional (also known as PBE0) [29,30] which is a hybrid generalized gradient approximation (GGA) method with a Hartree–Fock (HF) contribution of 25%. PBE1PBE functional was employed with triple-ζ basis set LANL2TZ+, which presents an addition diffuse *d* function, with Hay and Wadt effective core potential (ECP) for the Mn atom [31,32] and 6-31G(d,p) for all other atoms. Nevertheless, to assess the variations between the different DFT methodologies, some tests were performed on complex **1**. This set of tests also used a GGA functional method, BP86 [33], a hybrid meta-GGA, M06 [34], a double hybrid functional, B2-PLYP [35] and also the HF method. In addition, different basis sets were applied to the Mn atom, such as double-ζ LANL2DZ with ECP [31,32], the correlation consistent valence triple-ζ basis set with a Stuttgart–Dresden–Bonn fully relativistic effective core potential ECP10MDF [which will be referred in the text as VTZ-(ecp-10mdf)] [36,37] and also Weigend and Ahlrichs Def2-TVZP basis set [38] to whole system (see Supplementary material). Dichloromethane solvation effect was calculated with the continuous surface charge polarizable continuum model IEFPCM [39]. The solvation energy was evaluated by the difference between Gibbs free energy in solvent and the free energy in vacuum at 298 K, i.e., $\Delta G_{solvation} = \Delta G^{\circ}_{solvent} - \Delta G^{\circ}_{vacuum}$, where $\Delta G^{\circ}_{solvent}$ and $\Delta G^{\circ}_{vacuum}$ is the Gibbs free energy obtained after the optimization in solvent and vacuum, respectively. In addition, the isotropic polarizability (α) refers to the three diagonal elements of the polarizability tensor [$\alpha = (\alpha_{xx} + \alpha_{yy} + \alpha_{zz})/3$].

Transition energies and oscillator strengths were carried out with time-dependent-DFT (TD-DFT) method [40–44], using M06-2X functional [34]. TD-DFT approach was performed with optimized geometries in the solvent. TD-DFT was accomplished considering the first sixty excited states, although only selected electronic transitions were reported. Natural bond orbital (NBO) analysis was performed using the NBO6.0 program [45]. The natural population analysis (NPA) was employed in the charge distribution [46].

Table 1
Crystal data and structure refinement for [Mn(atc-Et)$_2$] (**3**).

Empirical formula	$C_{20}H_{26}MnN_8S_2$
Formula weight	497.55
Temperature	293(2) K
Wavelength	0.71073 Å
Crystal system	Monoclinic
Space group	$P2_1$
Unit cell dimensions	a = 8.83170(10) Å α = 90° b = 14.7684(3) Å β = 102.3330(10)° c = 9.3837(2) Å γ = 90°
Volume	1195.67(4) Å^3
Z	2
Density (calculated)	1.382 Mg/m^3
Absorption coefficient	0.751 mm^{-1}
F(000)	518
Crystal size	0.55 × 0.23 × 0.18 mm^3
Theta range for data collection	2.36 to 25.14°
Index ranges	−10 ≤ h ≤ 10, −17 ≤ k ≤ 17, −11 ≤ l ≤ 10
Reflections collected	7973
Independent reflections	4142 [R(int) = 0.0158]
Completeness to theta = 25.14°	99.5%
Absorption correction	Semi-empirical from equivalents
Max. and min. transmission	0.8767 and 0.6830
Refinement method	Full-matrix least-squares on F^2
Data/restraints/parameters	4142/1/284
Goodness-of-fit on F^2	1.026
Final R indices [I > 2sigma(I)]	R_1 = 0.0219, wR_2 = 0.0562
R indices (all data)	R_1 = 0.0228, wR_2 = 0.0567
Absolute structure parameter	0.037(11)
Largest diff. peak and hole	0.290 and −0.165 e.Å^{-3}

2.6. Determination of MICs

The anti-MTB activity of the compounds was determined by the REMA (Resazurin Microtiter Assay) method according to Palomino et al. [47]. Stock solutions of the tested compounds were prepared in DMSO and diluted in Middlebrook 7H9 broth (Difco) supplemented with oleic acid, albumin, dextrose and catalase (OADC enrichment — BBL/Becton-Dickinson), to obtain final drug concentration ranges of 0.09–25 μg/mL. The isoniazid was dissolved in distilled water and used as a standard drug. A suspension of the MTB $H_{37}Rv$ ATCC 27294 was cultured in Middlebrook 7H9 broth supplemented with OADC and 0.05% Tween 80. The culture was frozen at −80 °C in aliquots. After two days the CFU/mL of an aliquot was carried out. The concentration was adjusted by 5 × 10^5 UFC/mL and 100 μL of the inoculum was added to each well of a 96-well microtiter plate together with 100 μL of the compounds. Samples were set up in triplicate. The plate was incubated for 7 days at 37 °C. After 24 h 30 μL of 0.01% resazurin (solubilized in water) was added. The fluorescence of the wells was read after 24 h by TECAN Spectrafluor®.

2.7. Cytotoxicity assay

In vitro cytotoxicity assays (IC_{50}) were performed first on VERO epithelial cells (ATCC CCL81). This lineage is widely used for phenotypic screening of drugs to be regarded as a normal cell derived from normal human epithelial tissue. Following this approach, compounds with low cytotoxicity were investigated on the J774A.1 (ATCC TIB-67) murine macrophage cell line. The macrophages are the first cells of the immune response and also serve as reservoirs of MTB that can survive within these cells. Both studies are recommended by Pavan et al. [3]. The cells were routinely maintained in complete medium (DMEM for VERO and RPMI-1640 (VitroCell®) J774A.1) supplemented with 10% heat-inactivated fetal bovine serum (FBS) plus gentamicin (50 mg/L) and amphotericin B (2 mg/L), at 37 °C, in a humidified 5% CO_2 atmosphere. After reaching confluence, the cells were detached and counted. For the cytotoxicity assay, 1 × 10^5 cells/mL were seeded in 200 μL of complete medium in 96-well plates (NUNC^{tm}). The plates were incubated under the same conditions for 24 h, to allow cell adhesion prior to drug testing. The compounds were dissolved in DMSO (5%) and subjected to two-fold serial dilution from 500 to 3.9 μg/mL. The cells were exposed to the compounds at various concentrations for 24 h. Resazurin solution was then added to the cell cultures and incubated for 6 h. Cell respiration, as an indicator of cell viability, was detected by reduction of resazurin to resorufin, whose pink color and fluorescence indicate cell viability. A persistent blue color of resazurin is a sign of cell death. The fluorescence measurements (530 nm excitation filter and 590 nm emission filter) were performed in a SPECTRAfluor Plus (Tecan) microfluorimeter. The IC_{50} value was defined as the highest drug concentration at which 50% of the cells are viable relative to the control. Each test was set up in triplicate.

2.8. Selectivity Index

The selectivity index (SI) was calculated by dividing IC_{50} for the VERO cells by the MIC for the pathogen; if the SI is ≥10, the compound is then investigated further [48].

3. Results and discussion

3.1. Synthesis of the complexes

Reactions of Hatc-R with $MnCl_2 \cdot 2H_2O$ in the presence of Et_3N under reflux in MeOH afforded analytically pure microcrystalline precipitates of the manganese complexes **1**–**6** in reasonable yields (Scheme 1). The products are quite soluble in CH_2Cl_2 and DMSO but less soluble in methanol or ethanol. Elemental analyses are consistent with the formation of neutral complexes [Mn(atc-R)$_2$], in accordance with the molar conductivity values found, nearby 0 μS cm^{-1} in CH_2Cl_2.

3.2. Crystal structure of [Mn(atc-Et)$_2$] (**3**)

An ORTEP representation of **3** along with the numbering scheme is presented in Fig. 1. The crystal structure of the complex exhibits a 6-coordinated manganese(II) center bonded to two monoanionic atc-Et$^-$ ligands in *N*,*N*,*S*-tridentate mode. The metal is coordinated to the ligands through the pyridine nitrogen atoms N(1A) and N(1B), as well as the azomethine N(2A) and N(2B) atoms and the sulfur atoms S(1A) and S(1B), forming four six-membered chelate rings including the Mn(II) atom. The negative charge of the monoanionic thiosemicarbazonate is delocalized over the ligand moiety, through the conjugated double bond system, consistent with the single bond predominant character for the S – C bond the considerable double bond character observed for the C═N distances. Comparing the bond lengths found for complex **3** with those of the previously reported cationic complex [Mn(Hatc)$_2$]·(ClO$_4$)$_2$ [49], in which the thiosemicarbazone ligand (Hatc) remains protonated upon coordination, some differences are observed. A predominantly double C═S bond, bond distances of 1.671(8) and 1.679(8) Å, is found in [Mn(Hatc)$_2$]·(ClO$_4$)$_2$, while in **3** these values are 1.732(19) and 1.743(2) Å. The enlargement of the C – S bond in the monoanionic ligand is due to the deprotonation at N(3) followed by the thioenolization of the CS bond [21,49]. Furthermore, the tridentate ligands are nearly planar, almost perpendicular to each other, with N(1A) – Mn – N(1B) close to 90°. The S(1A) – Mn – S(1B) angle around 102° shows a clear distortion of the octahedral geometry. Additional information about bond lengths and angles for **3** can be found in Table 2.

The crystal of **3** is stabilized by intermolecular hydrogen bonds, as shown in Fig. 2. The nitrogen atom N(8) is H-bonded to the sulfur atom S(2b) of a symmetry related molecule, while N(7) interacts with a hydrogen atom bonded to atom N(4b) building a *zigzag* alignment of the complex molecules toward the direction [010].

3.3. Quantum chemical results

DFT calculations, based on the crystallographic data of complex **3**, were also performed. After optimization of structure **3**, the R groups on the thiosemicarbazone ligands were substituted and new optimizations were executed. For comparison with the XRD data, values for selected bond lengths and angles of the optimized structure of **3** were also inserted in Table 2. The perspective view of the optimized structure of **3** is presented in Fig. 1. The optimized structures of the other complexes can be found as supplementary material (Fig. SF1), while Table ST1 (Supplementary material) shows the geometric aspects and molecular properties. In regard to the comparison with the available experimental data, a difference of around 0.2 Å to Mn – S and 0.3 Å to Mn – N_{im} and Mn – N_{py} bond lengths between computed and experimental values is observed. These smaller bond lengths indicate an electron density increase in the metal–ligand bond orbitals, which may be a consequence of the quantum chemical simulations performed in vacuum. An explanation for this difference between the DFT and experimental values on metal–ligand bond lengths may be due to the hydrogen bonds formed in the crystal (see Fig. 2). Other DFT methods were also employed to verify the differences between the experimental and computational data. However an increase in the quality of the metal basis did not change the results considerably. These data are better discussed in the supplementary material quantum chemical analysis.

In order to understand the behavior of atomic charge distribution, the NPA method was employed [46]. Among the six thiosemicarbazone complexes, the manganese charge (qMn) ranges from 0.41 to 0.42. This charge sign is an important indicative of a σ donation from ligands to metal. Another interesting aspect is the small metal charge variation, which points out that the structural differences in the thiosemicarbazonate ligands used in this study did not affect the metal charge substantially. This absence of ligand effect in the atomic charge was also extended to the nitrogen and sulfur atoms, where the atomic charge was almost unaltered with the coordination of the different ligands. These results indicate that the atomic charge distribution toward the coordination sphere may not be an important aspect to understand the anti-MTB activity. On the other hand, observing the molecular electrostatic potential map of the six complexes (see Fig. SF2), slight changes are detected in the peripheral functional

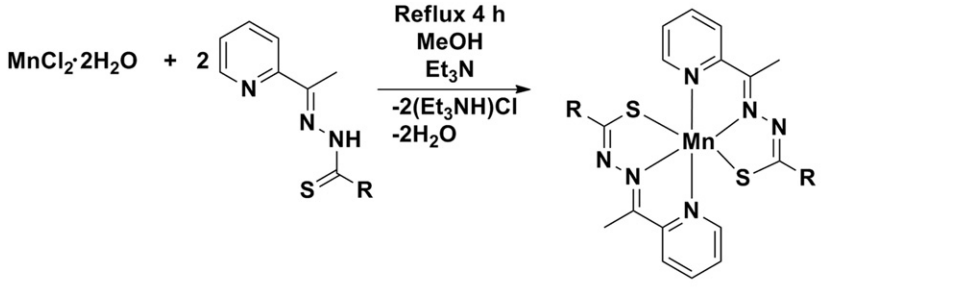

Scheme 1. Synthesis of the manganese(II) complexes.

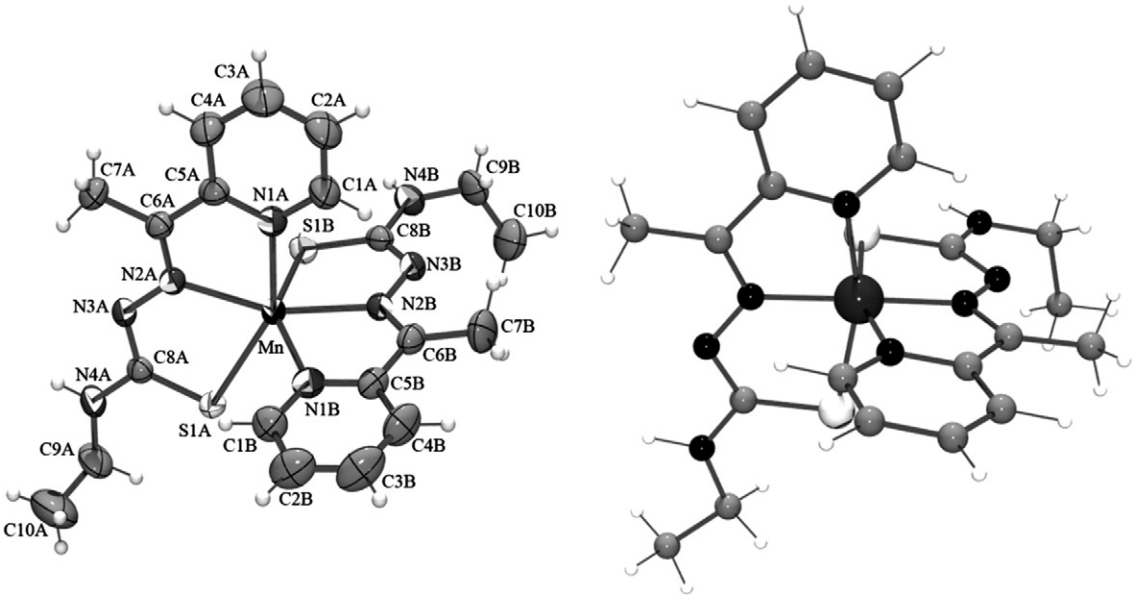

Fig. 1. ORTEP view (50% probability) and optimized structure of [Mn(atc-Et)$_2$] (**3**) with atom labels.

groups, with the exception of complex **6** where a large difference is observed, which may lead to a distinct biological activity.

Understanding the second order perturbation energy (E_2) allows the determination of the strength between donor and acceptor NBO, and gives some insights into the σ ligand donation to metal. An analysis of E_2 values shows that σ donation from nitrogen lone pair electrons to manganese ($_{LP}N \rightarrow Mn$) is approximately 418 kcal mol^{-1}, while in the case of the donation from sulfur lone pair electrons to manganese ($_{LP}S \rightarrow Mn$) it is around 35 kcal mol^{-1}, which is in accordance with the HSAB (hard and soft acids and bases) theory. Despite the fact that $_{LP}N \rightarrow Mn$ represents a contribution close to 8% of the total energy necessary to stabilize each thiosemicarbazone complex, $_{LP}S \rightarrow Mn$ consists of less than 1%. These values did not show high variations among the six complexes, which only points to the slight changes in the atomic charge distribution. Nevertheless, considering the strength of these interactions, a larger susceptibility for Mn – S bond dissociation can be emphasized in comparison to the Mn – N_{py} and Mn – N_{im} ones.

A TD-DFT analysis was also performed to understand the electronic transitions (see Table ST5). In experimental conditions, orange solutions are observed for the complexes in CH_2Cl_2 which display two intense bands within the regions 295–315 nm and 390–415 nm, similar to Groni et al. results [50]. The first band (295–315 nm) can be assigned as having predominantly a ligand–ligand charge transfer (LLCT) character, showing a ligand π → π* internal transition. Complex **4** is a distinct case, in which a minor metal to ligand charge transfer (MLCT), around 12%, is detected, referring to a $3d_{t2g} \rightarrow \pi^*_{CN}$ / π^*_{CC} transition. The second band among the complexes (390–415 nm) consists of a MLCT with particularly small contribution, ranging from 12 to 17%. For **5**, a third band is observed at 369.00 nm, corresponding to a major contribution from phenyl ring π–π* internal transitions. As expected, spin-forbidden *d–d* bands were not observed in the spectra of the high-spin d^5 Mn(II) complexes presented in this work.

Table 2
Selected bond lengths and angles (°) refined from X-ray and the optimized data in gas phase for **3** [PBE1PBE/Lanl2TZ+/6-31G(d,p)].

	XRD data for **3**	Calculated data for **3**
Bond lengths		
Mn – N(2A)/N(2B)	2.264(16)/2.254(15)	1.95011/1.93605
Mn – N(1A)/N(1B)	2.264(17)/2.280(15)	1.98394/1.98147
Mn – S(1A)/S(1B)	2.527(6)/2.521(5)	2.33386/2.33590
S(1A) – C(8A)/S(2A) – C(8B)	1.732(19)/1.743(2)	1.73553/1.72885
N(4A) – C(8A)/N(4B) – C(8B)	1.336(3)/1.347(3)	1.34581/1.34417
N(3A) – C(8A)/N(3B) – C(8B)	1.335(2)/1.321(3)	1.32209/1.32887
Bond angles		
N(2A) – Mn(1) – N(2B)	159.18(5)	177.02241
N(1B) – Mn(1) – N(1A)	90.48(6)	88.50337
S(1A) – Mn(1) – S(1B)	102.451(19)	95.37605
N(2A) – Mn(1) – N(1A)	71.73(6)	79.89498
N(2B) – Mn(1) – N(1B)	71.64(6)	79.72190
N(1A) – Mn(1) – S(1A)	145.24(5)	162.53870
N(1B) – Mn(1) – S(1B)	145.50(5)	162.30577
S(1A) – Mn(1) – N(2A)	76.01(4)	83.24206
S(1B) – Mn(1) – N(2B)	75.12(4)	83.22916
C(8A) – S(1A) – Mn(1)	97.56(6)	93.29756
C(8B) – S(1B) – Mn(1)	97.46(7)	93.26687

3.4. Infrared spectroscopy

The IR data are consistent with the *N,N,S*-coordination of the monoanionic ligands to the Mn(II) centers in the neutral complexes. The spectra of Hatc-R are characterized by two strong broad ν(NH) absorptions in the range of 3373–3203 cm^{-1}. For the complexes, only one band is observed in this region, according to the single deprotonation of the ligands. The very strong and sharp bands around 1580 cm^{-1}, assigned to ν(C═N) stretches in the ligands, appear at around 1590 cm^{-1} in the spectra of the complexes. The ν(C═S) bands at 846–800 cm^{-1} of the spectra of the free thiosemicarbazones are shifted to 773–788 cm^{-1} in the complexes.

3.5. Magnetic measurements and EPR studies

The oxidation state of the manganese central atom in the complexes was confirmed by measurements of the magnetic susceptibility. The values of magnetic moments measured at 20 °C, in the 5.90–6.55 BM range, are consistent with the calculated value of 5.9 BM, characteristic to d^5 high spin Mn(II) complexes.

The EPR spectra of Mn(II) complexes **1**–**6**, recorded from frozen DMSO solutions are depicted in Fig. 3. The spectra show the presence of two components for complexes **1**, **4** and **6**. The main component generates similar profiles for all complexes. The simulated spectrum shown in Fig. 3 corresponds to this species. The EPR parameters used to simulate it are g = [2.05 2.05 1.96] and D = 53.0 mT. The broad lines appear as a result of weak interactions between metal

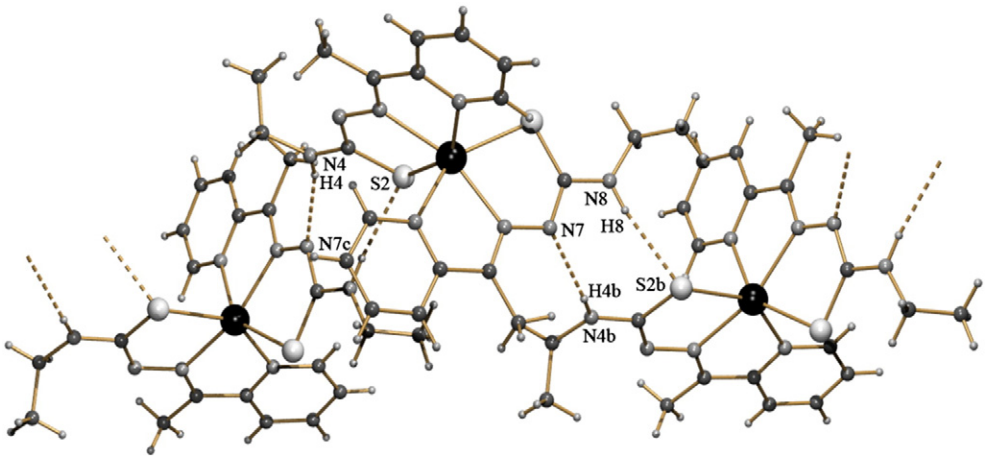

Fig. 2. Crystalline and molecular structure of [Mn(atc-Et)$_2$]. [N(8)···S(2b) = 3.3762(19) Å, N(8) – H(8)···S(2b) = 168.6°], [N(4)···N(7c) = 3.191(3) Å, N(4) – H(4)···N(7c) = 158.0°]. Symmetry operations used: (b) −x + 2, y − 1/2, −z + 2; (c) −x + 2, y + 1/2, −z + 2.

centers from neighbor molecules, interconnected by H-bonds, that are probably partially maintained in DMSO solution, as observed in the crystal structure of **3** (see Fig. 1), as described also for **5** [51]. Moreover, the minor components correspond to a monomeric species with D = 0 mT, showing the hyperfine structure of nuclear spin of manganese (I = 5/2), suggesting the binding of DMSO instead of donor atoms of the TSC ligands in the coordination sphere of the manganese centers. According to the quantum mechanical calculations performed, it is most probably that the DMSO molecule coordinates in positions originally occupied by sulfur atoms of the TSC ligands (see Section 3.3).

3.6. Electrochemical studies

Cyclic voltammetry (CV) and differential pulse voltammetry (DPV) of the complexes were performed in dichloromethane with PTBA as supporting electrolyte, in the potential range from 1.8 to −1.7 V. Due to the higher sensibility, the DPV results are shown in Table 3. All complexes presented the same behavior. Fig. 4A and B summarizes the CV and DPV, respectively, for compound **2**, exemplarily. For this complex, two well-defined quasi-reversible (i_{pa} / $i_{pc} \approx 1$) waves are detected. The two anodic processes correspond to the Mn(II)/Mn(III) and Mn(III)/Mn(IV) couples, while the two cathodic processes correspond to the Mn(IV)/Mn(III) and Mn(III)/Mn(II) couples. A cyclic voltammetry experiment with **2** was carried out in DMSO solution at room temperature and the redox potentials did not change, excluding the possibility of DMSO coordination, forming new species. Aiming to prove the presence of only one electron in the manganese compound processes, the processes were referenced to the standard ferrocene (Fig. 4C). The complexes presented here have an electrochemical behavior comparable to that observed for other manganese(II) complexes reported in the literature [52–54].

Through the values summarized in Table 3, it is possible to connect the redox potential with the R group bonded to the N(4) atom of the thiosemicarbazone ligand. It can be seen that the potential relative to the Mn(II)/Mn(III) couple became more positive with strongly electron-withdrawing R groups, according to the order: -methyl < -morpholinyl < -cyclohexyl < -ethyl < -H < phenyl, showing their influence on the Mn(II) center. Therefore it can be concluded that the phenyl group better stabilizes the oxidation state +II, while the methyl group, with electron donating capacity, better stabilizes the oxidation state +III. On the other hand, for the Mn(III)/Mn(IV) couple the potential order is somehow changed in relation to the first couple -methyl < -cyclohexyl < -ethyl < -H < -phenyl < -morpholinyl. It shows that the complex with the methyl group reaches the oxidation state +IV more easily than the other groups.

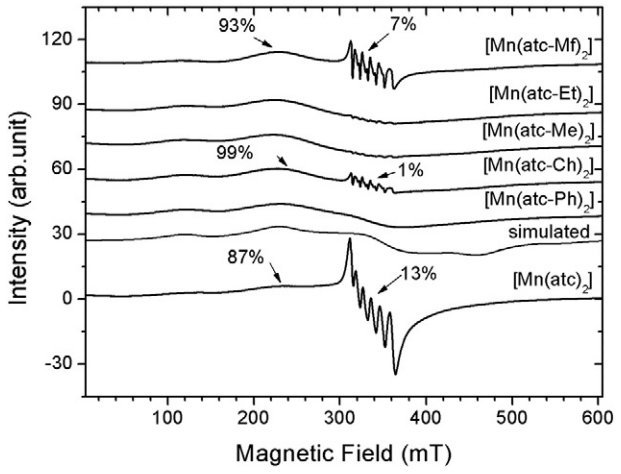

Fig. 3. Simulated and experimental EPR spectra of the [Mn(atc-R)$_2$] complexes from frozen DMSO solutions.

3.7. Biological activity

The biological activity of the compounds was evaluated by determining the values of MIC against the strains of *M. tuberculosis* H_{37}Rv ATCC 27294. Interesting results of MIC for synthetic compounds are values ≤12.5 μg/mL. They can then be further evaluated in cytotoxicity tests. VERO cells are more indicated to evaluate the cytotoxicity, which are epithelial and said to be normal. Tests against macrophage cell J774 complete the cytotoxicity tests, since they are cells of the immunologic system.

Table 3
Differential pulse data for the redox couples Mn(II)/Mn(III) and Mn(III)/Mn(IV) for all six complexes, measured in CH_2Cl_2 with 0.1 M PTBA as the electrolyte (all potentials referenced to the Fc/Fc^+ couple).

Complexes	$E_{Mn^{II}/Mn^{III}}$	$E_{Mn^{III}/Mn^{II}}$	$E_{1/2}$(V)	$E_{Mn^{III}/Mn^{IV}}$	$E_{Mn^{IV}/Mn^{III}}$	$E_{1/2}$(V)
1	0.36	0.38	0.37	0.96	0.99	0.98
2	0.19	0.20	0.19	0.83	0.86	0.84
3	0.30	0.26	0.28	0.96	0.96	0.96
4	0.27	0.25	0.26	0.93	0.88	0.91
5	0.37	0.40	0.39	0.97	1.01	0.99
6	0.24	0.24	0.24	1.00	1.00	1.00

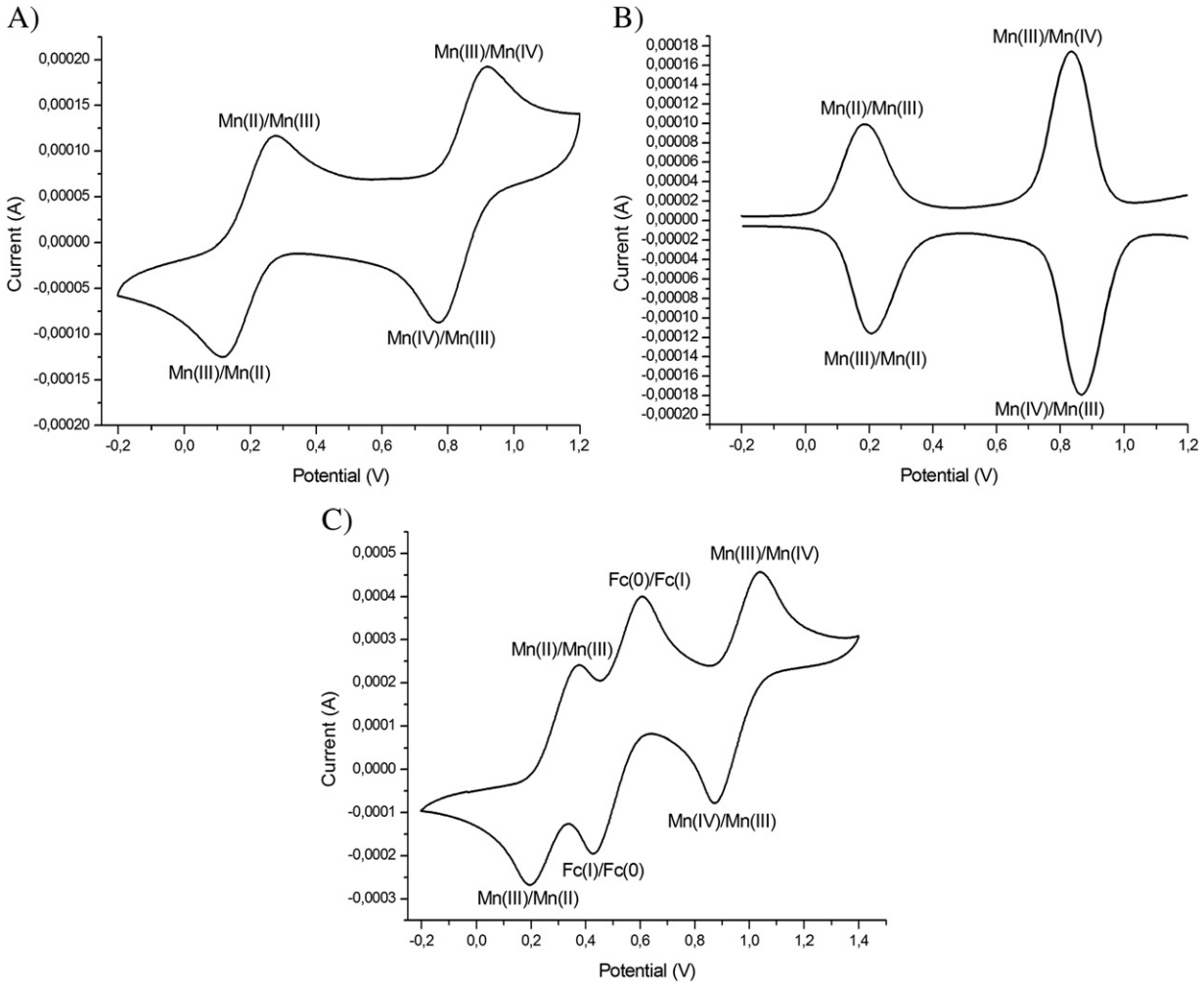

Fig. 4. (A) Cyclic voltammogram of [Mn(atc-Me)$_2$] (scan rate 100 mV s^{-1}) of and (B) differential pulse of [Mn(atc-Me)$_2$]. (C) Cyclic voltammogram of [Mn(atc-Me)$_2$] with the internal standard ferrocene. All measurements were carried out under argon atmosphere in solutions of CH_2Cl_2 (0.1 M [PTBA]) at a platinum electrode.

The biological results are shown in Table 4. From six manganese complexes, three showed MIC values lower than 10 μg/mL. As we know, structural changes in the ligand can alter significantly the activity [18]. Complexes **3** and **4** showed similar MIC (3.12 and 3.30 μg/mL, respectively) with low cytotoxicity of VERO cells (IC_{50} = 250 and 93.8 μg/mL, respectively) which characterizes these compounds as low toxic as seen at the high SI values. However, complex **4** was the only highly cytotoxic of J774A.1 cell. After the coordination of the ligands to the Mn(II) center, no clear trend in biological activity was observed. Most of the complexes show remarkable inhibitory effects. In the case of **1**–**4** and **6**, there was almost no significant change for MIC with respect to those of the previously published non-coordinated thiosemicarbazones [3]. However, complex **5** presents a considerably smaller MIC compared with the free ligand Hatc-Ph (15.6 μg/mL) [3]. This compound showed the lowest MIC and the highest IC_{50} among all tested compounds in this work. The calculation of the SI against VERO cells (SI > 641) shows the promising selectivity of this compound. We can compare these early results found for complex **5** with first line drugs such as isoniazid and rifampicin [55] as well as with new promising compounds such as PA-824, SQ-109 and even TMC 207 (Sirturo) [56], the first drug approved by FDA against MDR TB in the last 40 years. A classification of the manganese complexes in agreement with the increasing potential as anti-MTB agent, considering the SI values referred for VERO cells is **6** → **2** → **1** → **4** → **3** → **5**. As previously observed for vanadium(IV) thiosemicarbazone compounds [18], the most stable manganese complex, considering its participation in an oxidative process, was also the most active. Complex **5** is the most active complex and also presents the highest oxidation potential (see Table 4). The EPR results discussed above showed that in general the more stable complexes, considering the inertness about binding DMSO in coordination sites originally occupied by donor atoms of the thiosemicarbazonate ligands, are the most active. Besides, the manganese salt $MnCl_2 \cdot 2H_2O$ was not active up to 25 μg/mL.

Fig. 5 is arranged in a decreasing order of MIC values (increasing anti-MTB activity), which is an easy way to observe how the activity changes with the modifications of the R groups. Nickel complexes of

Table 4
Anti-MTB activity (MIC), cytotoxicity (IC_{50}), and selectivity index (SI) of the complexes.

Compounds	MIC		IC_{50}				SI[a]
			VERO		J774A.1		
	μg/mL	μM	μg/mL	μM	μg/mL	μM	IC_{50}/MIC
[Mn(atc)$_2$] (**1**)	18.2	41.22	500	1132.65	31.3	70.90	27.5
[Mn(atc-Me)$_2$] (**2**)	23.8	50.69	125	266.24	n.d.	n.d.	5.3
[Mn(atc-Et)$_2$] (**3**)	3.12	6.27	250	502.47	78.1	156.97	80.1
[Mn(atc-Ch)$_2$] (**4**)	3.3	5.44	93.8	154.85	<2	<3.30	28.4
[Mn(atc-Ph)$_2$] (**5**)	0.78	1.31	>500	>842.27	39.1	65.83	>641
[Mn(atc-Mf)$_2$] (**6**)	19.7	33.87	31.3	53.81	n.d.	n.d.	1.6
$MnCl_2 \cdot 2H_2O$	>25	–	–	–	–	–	–

[a] The selectivity index (SI) was calculated by the ratio IC_{50}(VERO)/MIC. n.d.: not determined.

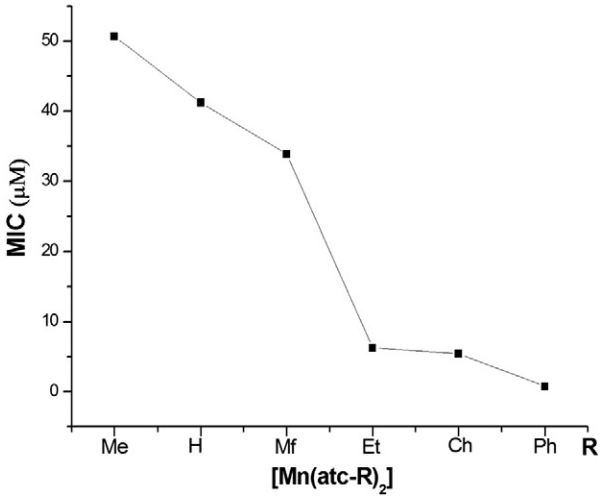

Fig. 5. Increasing order of anti-MTB activity (MIC) in relation to the peripheral thiosemicarbazonate groups (R).

the type [Ni(atc-R)$_2$] (R = Me, Ph) reported [19] presented similar MIC values as the analogous manganese complex [Mn(atc-Ph)$_2$] (**5**) presented here, but showing invariance of the activity with the different ligand substituents. High SI indexes are observed for analog complexes of both metals.

The use of a thiosemicarbazone manganese complex in a cocktail containing INH could possibly enhance the activation process of INH, since Mn(III) species formed by oxidation of Mn(II) species by KatG act as oxidants of the prodrug isoniazid [7], besides having its own activity, which could be effective in the treatment of tuberculosis.

4. Conclusions

A set of manganese compounds with thiosemicarbazones as ligands, varying the N(4) substituent group by H, methyl, ethyl, cyclohexyl, phenyl and morpholinyl, were synthesized in satisfactory yields and were fully characterized both in solution and in the solid state. The biological assays of these compounds showed early results better than first line drugs and even new promising anti-TB drugs. The high anti-MTB activity and the low cytotoxicity against eukaryotic cells show us a perfect "magic bullet". The coordination of thiosemicarbazones to the Mn(II) center may result in the enhancement of their anti-*M. tuberculosis* activities. Complex **5** is the one with the highest oxidation potential, suggesting that redox processes might also be related to the biological activity. The excellent activity of complex **5** may represent a novel strategy to prepare new antitubercular agents using manganese as metal center. Finally, these promising results encourage us to continue with this systematic investigation, modifying the ligand structure as well as the metal center in order to evaluate their role in the biological activity. Additionally, in vivo studies are underway in our laboratories to further evaluate these promising compounds. On the other hand, new investigations must be performed in order to know exactly the participation of the manganese in the bacterial inhibitory effect and to understand their mechanism of action.

Abbreviations

IC_{50}	half maximal inhibitory concentration
INH	isoniazid
CP (KatG)	catalase peroxidase
MDRTB	multidrug resistant tuberculosis
MIC	minimal inhibitory concentration
MTB	*Mycobacterium tuberculosis*
SI	selectivity index
TB	tuberculosis
TSC	thiosemicarbazone
DFT	density functional theory
TD-DFT	time-dependent-DFT
MLCT	metal to ligand charge transfer
LLCT	ligand–ligand charge transfer
Fc/Fc^+	ferrocene/ferricinium

Acknowledgments

The authors thank FAPESP (Grants 2009/54011-8, 2011/11593-7, 2011/16380-1), CNPq and CAPES for supporting this work. This work is also a collaboration research project of members of the Rede Mineira de Química (RQ-MG) supported by FAPEMIG (Project: REDE-113/10). R.B. Viana is grateful to the NCC/GridUNESP and CENAPAD/SP for the provision of computational facilities.

Appendix A. Supplementary data

CCDC 937108 contains the supplementary crystallographic data for **3**. These data can be obtained free of charge via http://www.ccdc.cam.ac.uk/conts/retrieving.html, or from the Cambridge Crystallographic Data Centre, 12 Union Road, Cambridge CB2 1EZ, UK; fax: (+44) 1223-336-033; or e-mail: deposit@ccdc.cam.ac.uk. Supplementary data associated with this article can be found, in the online version at http://dx.doi.org/10.1016/j.jinorgbio.2013.10.011.

References

[1] R.O. Pinheiro, E.B. de Oliveira, G. dos Santos, G.M. Sperandio da Silva, B.J. de Andrade Silva, R.M.B. Teles, A. Milagres, E.N. Sarno, M.P. Dalcolmo, E.P. Sampaio, Clin. Exp. Immunol. 171 (2013) 210–219.
[2] L.T. Daum, J.D. Rodriguez, S.A. Worthy, N.A. Ismail, S.V. Omar, A.W. Dreyer, P.B. Fourie, A.A. Hoosen, J.P. Chambers, G.W. Fischer, J. Clin. Microbiol. 50 (2012) 3831–3837.
[3] F.R. Pavan, P.I.S. Maia, S.R.A. Leite, V.M. Deflon, A.A. Batista, D.N. Sato, S.G. Franzblau, C.Q.F. Leite, Eur. J. Med. Chem. 45 (2010) 1898–1905.
[4] S. Sivendran, V. Jones, D. Sun, Y. Wang, A.E. Grzegorzewicz, M.S. Scherman, A.D. Napper, J.A. McCammon, R.E. Lee, S.L. Diamond, M. McNeil, Bioorg. Med. Chem. 18 (2010) 896–908.
[5] H.I. Lee, J.H. Yoon, J.S. Nam, Y.M. Kim, Y.T. Ro, J. Biochem. 147 (2010) 511–522.
[6] R.S. Magliozzo, J.A. Marcinkeviciene, J. Biol. Chem. 272 (1997) 8867–8870.
[7] M. Nguyen, A. Quémard, S. Broussy, J. Bernadou, B. Meunier, Antimicrob. Agents Chemother. 46 (2002) 2137–2144.
[8] R.F. Zabinski, J.S. Blanchard, J. Am. Chem. Soc. 119 (1997) 2331–2332.
[9] Z. Rahim, C. Nakajima, R. Raqib, K. Zaman, H.P. Endtz, A.G.M. van der Zanden, Y. Suzuki, Tuberculosis 92 (2012) 529–534.
[10] J. Oliveira, E.H.S. de Sousa, O.N. de Souza, I.S. Moreira, D.S. Santos, L.A. Basso, Curr. Pharm. Des. 12 (2006) 2409–2424.
[11] D. da G.J. Batista, P.B. da Silva, D.R. Lachter, R.S. Silva, R.Q. Aucelio, S.R.W. Louro, H. Beraldo, M. de N.C. Soeiro, L.R. Teixeira, Polyhedron 29 (2010) 2232–2238.
[12] P.I.S. Maia, A. Graminha, F.R. Pavan, C.Q.F. Leite, A.A. Batista, D.F. Back, E.S. Lang, J. Ellena, S.S. de Lemos, H.S. Salistre-de-Araujo, V.M. Deflon, J. Braz. Chem. Soc. 21 (2010) 1177–1186.
[13] P.I.S. Maia, H.H. Nguyen, D. Ponader, A. Hagenbach, S. Bergemann, R. Gust, V.M. Deflon, U. Abram, Inorg. Chem. 51 (2012) 1604–1613.
[14] X.F. Zhu, Y.H. Fan, Q. Wang, C.L. Chen, M.X. Li, J.W. Zhao, J. Zhou, Russ. J. Coord. Chem. 38 (2012) 478–483.
[15] R.A. de Souza, A. Stevanato, O. Treu-Filho, A.V.G. Netto, A.E. Mauro, E.E. Castellano, I.Z. Carlos, F.R. Pavan, C.Q.F. Leite, Eur. J. Med. Chem. 45 (2010) 4863–4868.
[16] D. Santos, B. Parajón-Costa, M. Rossi, F. Caruso, D. Benítez, J. Varela, H. Cerecetto, M. González, N. Gómez, M.E. Caputto, A.G. Moglioni, G.Y. Moltrasio, L.M. Finkielsztein, D. Gambino, J. Inorg. Biochem. 117 (2012) 270–276.
[17] D.R. Richardson, D.S. Kalinowski, V. Richardson, P.C. Sharpe, D.B. Lovejoy, M. Islam, P.V. Bernhardt, J. Med. Chem. 52 (2009) 1459–1470.
[18] P.I. da S. Maia, F.R. Pavan, C.Q.F. Leite, S.S. Lemos, G.F. de Sousa, A.A. Batista, O.R. Nascimento, J. Ellena, E.E. Castellano, E. Niquet, V.M. Deflon, Polyhedron 28 (2009) 398–406.
[19] P.I.S. Maia, F.R. Pavan, C.Q.F. Leite, U. Abram, E.S. Lang, A.A. Batista, V.M. Deflon, in: L. Pele, J.J. Powell, S. Kinrade, R. Jugdaohsingh, P. Collery, I. Maymard, A. Badawi (Eds.), Metal Ions in Biology and Medicine and Aqueous Chemistry and Biochemistry of Silicon, John Libbey Eurotext, Paris, 2011, pp. 164–171.
[20] M.X. Li, C.L. Chen, D. Zhang, J.Y. Niu, B.S. Ji, Eur. J. Med. Chem. 45 (2010) 3169–3177.
[21] M.X. Li, D. Zhang, L.Z. Zhang, J.Y. Niu, B.S. Ji, Inorg. Chem. Commun. 13 (2010) 1572–1575.
[22] M. Joseph, V. Suni, C.R. Nayar, M.R.P. Kurup, H.-K. Fun, J. Mol. Struct. 705 (2004) 63–70.

[23] M.A. Soares, J.A. Lessa, I.C. Mendes, J.G. Da Silva, R.G. dos Santos, L.B. Salum, H. Daghestani, A.D. Andricopulo, B.W. Day, A. Vogt, J.L. Pesquero, W.R. Rocha, H. Beraldo, Bioorg. Med. Chem. 20 (2012) 3396–3409.
[24] A. Earnshaw, Introduction to Magnetochemistry, Academic Press, New York, 1968.
[25] O. Kahn, Molecular Magnetism, VCH Publishers, 1993.
[26] G.M. Sheldrick, SHELXS97, Program for the Solution of Crystal Structures, University of Göttingen, Germany, 1997.
[27] G.M. Sheldrick, SHELXL97, Program for the Refinement of Crystal Structures, University of Göttingen, Germany, 1997.
[28] M. Frisch, G. Trucks, H. Schlegel, G. Scuseria, M. Robb, J. Cheeseman, J. Montgomery, T. Vreven, K. Kudin, J. Burant, J. Millam, S. Iyengar, J. Tomasi, V. Barone, B. Mennucci, M. Cossi, G. Scalmani, N. Rega, G. Petersson, H. Nakatsuji, M. Hada, M. Ehara, K. Toyota, R. Fukuda, J. Hasegawa, M. Ishida, T. Nakajima, Y. Honda, O. Kitao, H. Nakai, M. Klene, X. Li, J. Knox, H. Hratchian, J. Cross, V. Bakken, C. Adamo, J. Jaramillo, R. Gomperts, R. Stratmann, O. Yazyev, A. Austin, R. Cammi, C. Pomelli, J. Ochterski, P. Ayala, K. Morokuma, G. Voth, P. Salvador, J. Dannenberg, V. Zakrzewski, S. Dapprich, A. Daniels, M. Strain, O. Farkas, D. Malick, A. Rabuck, K. Raghavachari, J. Foresman, J. Ortiz, Q. Cui, A. Baboul, S. Clifford, J. Cioslowski, B. Stefanov, G. Liu, A. Liashenko, P. Piskorz, I. Komaromi, R. Martin, D. Fox, T. Keith, A. Laham, C. Peng, A. Nanayakkara, M. Challacombe, P. Gill, B. Johnson, W. Chen, M. Wong, C. Gonzalez, J. Pople, Gaussian 03, Revision C.02, 2003.
[29] J.P. Perdew, K. Burke, M. Ernzerhof, Phys. Rev. Lett. 77 (1996) 3865–3868.
[30] C. Adamo, V. Barone, J. Chem. Phys. 110 (1999) 6158.
[31] P.J. Hay, W.R. Wadt, J. Chem. Phys. 82 (1985) 299.
[32] L.E. Roy, P.J. Hay, R.L. Martin, J. Chem. Theory Comput. 4 (2008) 1029–1031.
[33] J.P. Perdew, Phys. Rev. B 33 (1986) 8822–8824.
[34] Y. Zhao, D.G. Truhlar, Theor. Chem. Acc. 120 (2007) 215–241.
[35] S. Grimme, J. Chem. Phys. 124 (2006) 034108.
[36] M. Dolg, U. Wedig, H. Stoll, H. Preuss, J. Chem. Phys. 86 (1987) 866.
[37] J.M.L. Martin, A. Sundermann, J. Chem. Phys. 114 (2001) 3408.
[38] F. Weigend, R. Ahlrichs, Phys. Chem. Chem. Phys. 7 (2005) 3297.
[39] G. Scalmani, M.J. Frisch, J. Chem. Phys. 132 (2010) 114110.
[40] M.E. Casida, C. Jamorski, K.C. Casida, D.R. Salahub, J. Chem. Phys. 108 (1998) 4439–4449.
[41] R.E. Stratmann, G.E. Scuseria, M.J. Frisch, J. Chem. Phys. 109 (1998) 8218–8224.
[42] C. Van Caillie, R.D. Amos, Chem. Phys. Lett. 308 (1999) 249–255.
[43] F. Furche, R. Ahlrichs, J. Chem. Phys. 117 (2002) 7433.
[44] G. Scalmani, M.J. Frisch, B. Mennucci, J. Tomasi, R. Cammi, V. Barone, J. Chem. Phys. 124 (2006) 094107.
[45] E.D. Glendening, J.K. Badenhoop, A.E. Reed, J.E. Carpenter, C.M. Bohmann, C.M. Morales, C.R. Landis, F. Weinhold, NBO 6.0, Theoretical Chemistry Institute, University of Wisconsin, Madison, 2013.
[46] A.E. Reed, R.B. Weinstock, F. Weinhold, J. Chem. Phys. 83 (1985) 735.
[47] J.C. Palomino, A. Martin, M. Camacho, H. Guerra, J. Swings, F. Portaels, Antimicrob. Agents Chemother. 46 (2002) 2720–2722.
[48] T.D.S. Program, Antimicrob. Agents Chemother. 45 (2001) 1943–1946.
[49] L. Liu, W. Shi, X.Y. Chen, Y.L. Chen, P. Cheng, Synth. React. Inorg. Met. 36 (2006) 549–554.
[50] S. Groni, C. Hureau, R. Guillot, G. Blondin, G. Blain, E. Anxolabéhère-Mallart, Inorg. Chem. 47 (2008) 11783–11797.
[51] T.D. Tzima, G. Sioros, C. Duboc, D. Kovala-Demertzi, V.S. Melissas, Y. Sanakis, Polyhedron 28 (2009) 3257–3264.
[52] A. Neves, S.M.D. Erthal, I. Vencato, A.S. Ceccato, Y.P. Mascarenhas, O.R. Nascimento, M. Horner, A.A. Batista, Inorg. Chem. 31 (1992) 4749–4755.
[53] R.A. Lewis, G. Wu, T.W. Hayton, Inorg. Chem. 50 (2011) 4660–4668.
[54] N.E. Chakov, M. Soler, W. Wernsdorfer, K.A. Abboud, G. Christou, Inorg. Chem. 44 (2005) 5304–5321.
[55] G. Alliance, T.B.D. Development, B. Street, Handbook of Anti-tuberculosis Agents, N. York, 88, 2008, pp. 85–170.
[56] R. Osborne, Nat. Biotechnol. 31 (2013) 89–91.